11th Annual Space Traffic Management Conference – STM 2025
04-05 March, 2025, Austin, TX, USA

IAA-STM-25-24-029

DEFINING ORBITAL CAPACITY THROUGH OPERATIONAL FEASIBILITY

William E. Parker*, Maya Harris†, Giovanni Lavezzi‡, and Richard Linares§
Department of Aeronautics and Astronautics, Massachusetts Institute of Technology, Cambridge, MA 02139, USA

Defining an upper limit on sustainable satellite activity is crucial for managing and sharing Earth's orbital environment. Orbital carrying capacity quantifies the distribution of satellites that can sustainably operate within a given regime, providing a practical upper bound on space traffic. These capacity solutions are generally driven by constraints that reflect the quantities we seek to sustain. Previous efforts have primarily focused on preventing unstable debris growth leading to Kessler syndrome. However, even in a dynamically stable environment with no cascading debris growth, an orbit may still be operationally infeasible if conjunctions requiring risk mitigation action are too frequent for practical use. In this work, an operational feasibility constraint is introduced to quantify the operational capacity. A constraint is imposed that limits the number of acceptable satellite conjunctions per month. The entire public catalog of tracked objects in Low Earth Orbit is used to identify conjunction nodes, calculated according to Keplerian dynamics, with individual objects characterized by their total conjunction frequency. This framework provides a consistent method for defining operational criticality, occupation, and capacity in the same interpretable units, offering a new approach to tracking space sustainability that complements existing metrics.

Keywords: Capacity, operations, conjunction assessment

*Ph.D. student, *wparker@mit.edu.*
†Graduate student, *mharris4@mit.edu.*
‡Postdoctoral Associate, *glavezzi@mit.edu.*
§Associate Professor, *linaresr@mit.edu.*

I. Introduction

The concept of carrying capacity originated in conservation ecology to describe the maximum number of individuals an environment can indefinitely sustain without degradation [1]. The carrying capacity of any system is determined by constraints, which vary depending on what exactly we seek to sustain. In recent years, space sustainability advocates have developed measures of orbital carrying capacity to establish thresholds on space activity that would prevent long-term degradation of the space environment. Despite these significant efforts, a unified definition of orbital capacity, and a consensus on how to measure current populations' occupation of that capacity remain elusive within the industry. This lack of consensus stems, in part, from differing interpretations of sustainability and the selection of constraints used to define sustainable limits on space activity. While many constraints could feasibly be applied to orbital capacity, various stakeholders prioritize these constraints differently, leading to divergent assessments.

Much of the existing work on orbital capacity focuses on the dynamical stability of the space environment [2–5]. Such frameworks aim to avoid a Kessler syndrome scenario by constraining populations based on collision rates, object counts, object mass, and other related characteristics. However, additional constraints—such as launch rate limitations, spectrum availability [6], radio and optical interference for terrestrial astronomy [7], ground safety risk [8], and atmospheric pollution during satellite launch [9] and reentry [10]—also impose practical limits on space activity that should be considered in capacity estimates, but are often neglected.

Ultimately, the selection of appropriate constraints depends on the specific objective. If the primary goal is to avoid a cascading debris scenario, dynamical stability should be prioritized. If, instead, sustained operational feasibility is prioritized, the constraint should be determined by a collision risk threshold beyond which operators deem missions infeasible. Because different capacity constraints may be active in different orbital regions, the true overall capacity is determined by the most restrictive constraint in each region. Furthermore, each constraint typically requires independent analysis to identify viable capacity solutions. This work explicitly explores operational feasibility as a constraint for defining the satellite carrying capacity of Earth's orbital space to complement existing dynamical stability constraints.

Most previous orbital sustainability assessments overlook the impact of *entropy* on capacity. Structured satellite deployments—common in large constellations—along with enhanced space domain awareness and advanced collision avoidance technologies can enable safer operation in densely occupied regions, provided the supporting infrastructure is highly robust. Disordered, uncoordinated satellite trajectories lead to regular conjunctions that require burdensome mitigation action. However, few existing orbital capacity metrics explicitly account for varying levels of structure in orbital populations,

limiting their ability to model the key enablers for sustainable space activity. This work explicitly takes entropy into account by considering realistic orbital mechanics and identifying structure relationships between object populations.

Operational feasibility is constrained using nominal conjunction frequencies from low-fidelity analytical orbit propagation. A Keplerian dynamics assumption enables efficient screening of conjunction nodes and revisit frequencies across the entire LEO catalog in minutes. Objects are ranked by conjunction frequency, with the top 15 listed for further analysis. An upper limit of 10 conjunctions per month is imposed, as more frequent collision risk mitigation would be impractical for most operators.

The paper is organized as follows. Section II discusses the importance of reaching a consensus on the definitions of orbital capacity, criticality, and occupation. Section III discusses the current state-of-the-art of space evolutionary models with a focus on their limitations. Section IV introduces the operationally feasible capacity framework. Section V presents the results from an analysis of the existing population in LEO. Lastly, final remarks to conclude the paper are provided in Section VI.

II. Distinguishing Capacity, Criticality, and Occupation

Current regulations and guidelines encourage individual satellite operators to follow sustainable best practices to minimize their impact on the orbital environment [11]. However, even if every satellite adheres to these principles, their collective presence can still degrade the environment. While a bottom-up approach—where sustainability is promoted by reducing the environmental impact of each individual satellite—helps mitigate harm, it does not address the inherently collective nature of the problem. Sustainability in orbit requires coordination and system-wide constraints, not just responsible individual behavior. A truly sustainable framework must derive satellite impact from top-level environmental constraints on capacity, ensuring that each satellite's contribution is assessed in the context of the broader system. Without establishing an upper limit on sustainable space activities, stakeholders cannot determine whether current or future satellite populations remain within sustainable bounds.

Similar issues of identifying the impact of individuals on a large-scale problem exist in addressing climate change. The 2015 Paris Agreement established a global goal to reduce increases in global temperature to 1.5°C above pre-industrial levels to prevent the worst impacts of climate change [12]. This threshold provides policymakers, organizations, and individuals with a clear benchmark against which to measure the contribution of their small-scale actions to the problem as a whole. Similarly, space sustainability requires well-defined thresholds to identify and mitigate critical tipping points in Earth's orbit. Without such limits, there is no effective way to proactively prevent long-term degradation of the orbital environment.

Part of the problem in space sustainability is the lack of clear and consistent vocabulary. The terms *capacity* and *criticality* are used inconsistently and sometimes interchangeably. Capacity should refer to constraint-driven limits on sustainable space activity that quantify the amount of orbital resource that is available. *Criticality* is a measure of a spacecraft's (or a population's) impact on the space environment. Most space sustainability metrics that have been developed so far are criticality metrics; they often combine different properties of a spacecraft (i.e. mass, cross-sectional area, orbit parameters, local object density, etc.) and produce a metric that is proportional to the amount of risk the spacecraft presents to the surrounding environment [13–15]. While these metrics are very useful for comparing the *relative* impact of different satellites on their environment, they do not correlate directly to capacity, which is defined by environmental constraints. Several efforts have focused on defining capacity by extending criticality metrics to the population-level [16], but these approaches often fail to capture the constraint-driven nature of rigorous capacity assessments.

The term *occupation* is rarely used in assessments of orbital sustainability but is essential for distinguishing between key variables in the broader space sustainability framework. Occupation serves as the complement to capacity, representing how much of the available orbital resource is currently being utilized. While capacity is influenced by environmental variability, such as long-term climate change in the thermosphere [17], occupation can be actively managed through sustainable best practices by satellite operators. In other words, while the total available orbital resource is largely fixed, its efficient use can be optimized through coordination and sustainability measures that minimize unnecessary occupation. For example, satellite collision avoidance does not alter capacity but does reduce occupation. For these distinctions to be meaningful, capacity should not be measured simply as the number of satellites but rather in terms that reflect the system's fundamental constraints.

To ensure clear interpretation of individual impacts on the overall system, capacity, criticality, and occupation must be measured in consistent units. Establishing interpretable, standardized metrics is crucial for enabling regulators, operators, and the public to accurately assess risks and implement effective strategies for sustainable space operations.

III. Limitations of Evolutionary Modeling

Predicting the long-term evolution of the space debris environment and assessing orbital capacity rely on computational models that capture the complex dynamics of space object populations. These evolutionary models seek to simulate the temporal evolution of space object populations and their interactions, to understand the sustainability of space activities, to inform effective mitigation strategies, and to test the

long-term effects of space sustainability metrics. Within evolutionary modeling, two prominent methodologies emerge: Source-Sink Evolutionary Models (SSEMs) and Monte Carlo (MC) methods.

SSEMs [18–23] offer a computationally efficient approach by representing the space environment as a series of interconnected altitude shells and tracking the population of different object species within these shells. Grouping objects into species with similar characteristics, SSEMs usually employ kinetic gas theory to estimate collision probabilities within these shells, assuming a homogeneous distribution of objects for simplification. This approach allows for rapid simulations and is particularly useful for capturing global trends in debris evolution and exploring policy implications through scenario analysis [24–26]. However, SSEMs, due to their reliance on kinetic gas theory, inherently simplify collision dynamics, neglecting the spatial structure and non-uniformities of real debris distributions. This simplification, while enabling computational speed, compromises model fidelity and may lead to an underestimation of localized collision risks and the complex orbital behavior of objects, and the true collision risk is significantly underestimated.

MC methods [27–37], in contrast, while they can rely on the kinetic gas theory to determine the probability of collisions, provide a higher fidelity representation by simulating the trajectory of individual space objects, explicitly tracking their states and interactions. This individual object tracking allows MC models to capture the spatial structure of debris clouds and more accurately model collision dynamics, offering a more accurate prediction of the debris evolution. However, the increased fidelity of MC methods comes with a significant computational burden. Propagating millions of objects over extended periods demands substantial computing resources and time, making them less practical for rapid analyses, iterative design processes, or broad policy explorations. Furthermore, MC models exhibit a heightened sensitivity to input parameters, particularly to the uncertainties inherent in space weather predictions, necessitating multiple simulations to achieve statistically robust results and further increasing computational demands. While MC methods offer a more realistic portrayal of the space environment, their computational intensity and input sensitivity make them less practical for routine capacity assessments and rapid decision support.

Another limitation affecting all space debris models is the inherent uncertainty in modeling atmospheric drag in LEO [38]. As highlighted in [39], the atmospheric density, the primary driver of drag, is subject to substantial variability influenced by solar activity and geomagnetic storms, which are themselves difficult to predict with accuracy over long timescales. Bowman et al. [40] acknowledge the complexities of empirical atmospheric models like JB2008, which, despite improvements, still rely on extrapolated historical data that cannot fully capture the dynamic and unpredictable nature of the

thermosphere. This uncertainty, as Lewis et al. [29] emphasize, directly translates into significant uncertainties in long-term debris population projections, as drag is the primary natural mechanism for debris removal in LEO. Consequently, even the most sophisticated MC models are ultimately constrained by the fundamental unpredictability of atmospheric drag.

IV. The Operationally Feasible Capacity

A. Conjunction Screening and Nodes

Conjunction screening, the process of searching for potential conjunctions days in advance to avoid satellite collisions [41], has familiar requirements for capturing realistic satellite dynamics while retaining low computational cost. Realistic dynamics are important because the screening step is meant to identify candidate conjunctions for detailed inspection and follow-up. Low computational cost is important because the screening needs to be done regularly (several times per day) on the entire tracked catalog of objects. A key insight to be learned from the conjunction screening process is that collision risk is not uniform in time or space. For any pair of tracked objects there is at maximum two potential conjunction nodes – or orbital crossings. A collision between any two objects of interest is impossible if the objects are not near the conjunction nodes. Figure 1 shows the three potential orbital geometries that would result in zero, one, or two conjunction nodes for a pair of tracked objects.

In conjunction screening, this concept of conjunction nodes helps to reduce the number of events that require computationally expensive high-fidelity orbital propagation analysis. The first pass check on potential conjunctions can be done with an assumption of Keplerian dynamics using the last issued TLEs for each object of interest. Once the conjunction nodes are identified, each can be analyzed based on the proximity of the conjunction and the orbit phasing of the satellites.

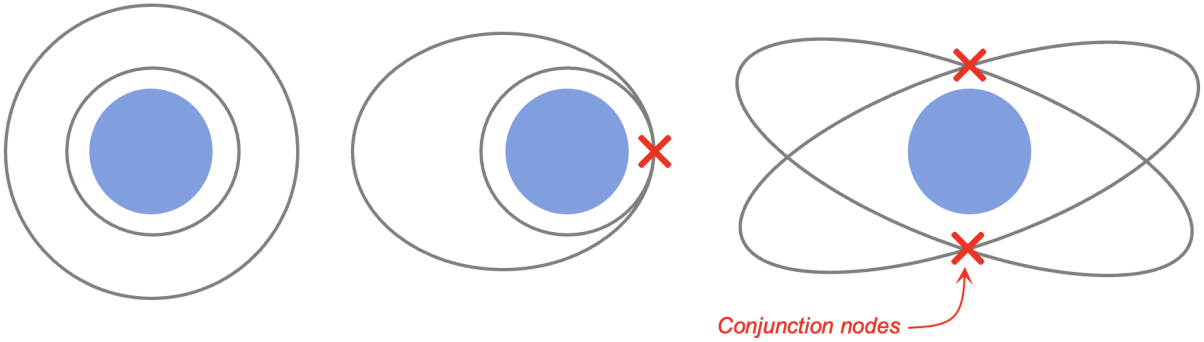

Fig. 1 Examples of orbital geometries resulting in zero, one, or two conjunction nodes.

B. Constraining Conjunction Frequency

The general procedure for the operationally feasible capacity framework is defined in Algorithm 1. The following steps are used to execute this algorithm. For each pair of tracked objects, we first identify their respective perigee and apogee radii according to

$$r_p = a(1-e) \tag{1}$$

$$r_a = a(1+e) \tag{2}$$

where a is the semi-major axis of the orbit and e is the eccentricity. A conjunction between a pair of objects A and B may only occur if their altitude ranges overlap somewhere, or when

$$\max(r_p^A, r_p^B) \leq \min(r_a^A, r_a^B). \tag{3}$$

If that condition is met, then we begin the procedure for identifying potential conjunctions. Computing the conjunction nodes for any two objects subject to Keplerian dynamics is straightforward from the basic equations of motion. The normal vector to the orbital plane is initially computed using each satellite's inclination (i) and right ascension of the ascending node (Ω).

The normal vector $\mathbf{n}$ for each pair of objects is given by:

$$\mathbf{n}_1 = \begin{bmatrix} \sin(\Omega_1)\sin(i_1) \\ -\cos(\Omega_1)\sin(i_1) \\ \cos(i_1) \end{bmatrix}, \quad \mathbf{n}_2 = \begin{bmatrix} \sin(\Omega_2)\sin(i_2) \\ -\cos(\Omega_2)\sin(i_2) \\ \cos(i_2) \end{bmatrix}. \tag{4}$$

Algorithm 1 Operationally Feasible Capacity Framework

Input: Catalog of objects with orbital elements from their latest TLEs.
for each unique pair of objects (A,B) in the TLE catalog **do**
  if $\max(r_p^A, r_p^B) \leq \min(r_a^A, r_a^B)$ **then**
    Identify the line of intersection of their orbital planes (or identify if they are coplanar).
    if orbital distances on the line of intersection are within 100 m **then**
      Compute the common period T_c, the time between conjunctions (should they occur).
      Check whether a conjunction occurs within T_c given the initial orbit phasing.
      if a conjunction occurs within T_c **then**
        Record the conjunction node and nodal conjunction frequency $(T_c)^{-1}$.
      end if
    end if
  end if
end for
for each satellite in the catalog **do**
  Sum the satellite's nodal conjunction frequencies f_c^n to compute the satellite conjunction frequency f_c^s.
  if satellite conjunction frequency > 10 conjunctions per month **then**
    Flag the satellite/orbit for further investigation.
  end if
end for

Given the normal vectors of two orbital planes, $\mathbf{n}_1$ and $\mathbf{n}_2$, the unit vector $\hat{\mathbf{m}}$ of the line of intersection is computed as:

$$\hat{\mathbf{m}} = \frac{\mathbf{n}_1 \times \mathbf{n}_2}{\|\mathbf{n}_1 \times \mathbf{n}_2\|} \tag{5}$$

where $\times$ denotes the cross product and $\|\cdot\|$ is the L_2 norm. The next step is to compute the orbital radii along $\hat{\mathbf{m}}$ where the satellites' orbit planes intersect. The radius r of a satellite from the focus is given by the Keplerian orbital equation

$$r = \frac{a(1-e^2)}{1+e\cos(\nu)} \tag{6}$$

where ν is the true anomaly of the orbit. The apse line or direction of periapsis, $\hat{\mathbf{p}}$, is

$$\hat{\mathbf{p}} = \frac{\mathbf{e}}{\|\mathbf{e}\|} \tag{7}$$

The angle ϕ between the intersection line $\hat{\mathbf{m}}$ and the apse line is calculated as

$$\phi = \arccos\left(\hat{\mathbf{m}} \cdot \hat{\mathbf{p}}\right). \tag{8}$$

For each direction along $\hat{\mathbf{m}}$, we compute the distance from the focus substituting ϕ for ν in Eq. 6. Thus, the position vectors of the closest approach points between the orbits are then

$$\begin{aligned}
\mathbf{r}_1^A &= r^A(\phi) \cdot \hat{\mathbf{m}} \\
\mathbf{r}_2^A &= r^A(-\phi) \cdot -\hat{\mathbf{m}} \\
\mathbf{r}_1^B &= r^B(\phi) \cdot \hat{\mathbf{m}} \\
\mathbf{r}_2^B &= r^B(-\phi) \cdot -\hat{\mathbf{m}}.
\end{aligned} \tag{9}$$

A conjunction node is identified when $\sqrt{\left(\mathbf{r}_1^A - \mathbf{r}_1^B\right)^2} < \varepsilon$ or $\sqrt{\left(\mathbf{r}_2^A - \mathbf{r}_2^B\right)^2} < \varepsilon$, where $\varepsilon = 100$ m in this work.

The procedure above is repeated for every pair of tracked satellites. For each pair, the positions of the closest orbital approach points are computed and stored. A conjunction node is only identified if the orbital crossing is within ε. Every conjunction node has a characteristic nodal conjunction frequency – which determines the rate at which the two satellites conjoin at the node. This nodal conjunction frequency is equivalent to the least common multiple (LCM) of the orbit periods for the pair of satellites conjoining at the node. This *common period*, T_c, measures the time between conjunctions at a conjunction node. It should not be confused with the synodic period, which measures the amount of time it takes for two objects to return to a reference orbit phasing. The common period enforces a requirement that an integer number of orbit

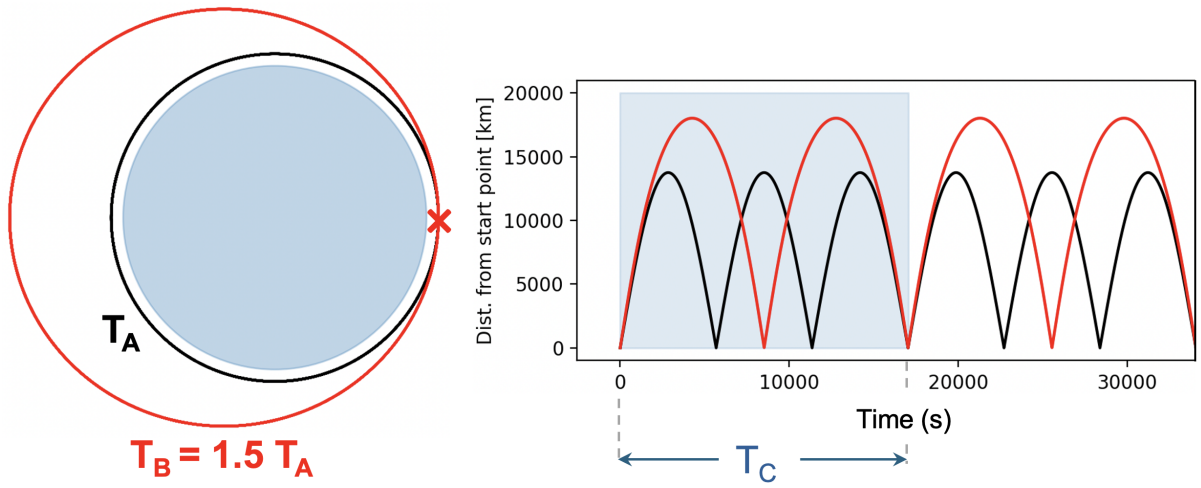

Fig. 2 T_c represents the period between conjunctions for any pair of objects. The figure depicts a simple example where T_B = 1.5 T_A.

periods has passed for each object, while the synodic period does not. T_c is found by:

$$T_c = qT_A = pT_B, \quad \text{where } p,q \in Z. \tag{10}$$

T_A and T_B are the orbital periods for satellites A and B, respectively. The closest rational approximation for p and q is found within a tolerance (10^{-3} in this case, which enforces that the orbit crossings are within $\sim$1 s). Figure 2 shows that T_c is equivalent to the conjunction frequency at a conjunction node of interest. For a given primary object, secondary objects with orbit periods that are integer multiples of the primary's orbit period are in resonance. For example, two satellites that belong to a constellation may operate at the same orbit altitude but different planes, and thus would likely share two conjunction nodes. Those satellites will generally have close to a 1:1 resonance, meaning that if their orbits are properly maintained, their nodal crossings should be naturally de-conflicted. For satellite pairs not de-conflicted by design, it is possible to experience *repeat conjunctions* – regular close approaches that cause a significant burden on conjunction assessment and collision avoidance systems. The conjunction frequency for each node, f_c^n, is equivalent to the inverse of the common period, $(T_c)^{-1}$.

In many cases, satellite pairs can go their entire common period without colliding. Since their orbital configuration resets after T_c, this is generally an indication that those objects should never collide (according to the simplified Keplerian dynamics). In this work, only conjunctions in which satellites cross the conjunction node within a time interval $\Delta t_{1-2} \leq 1$ second of each other are deemed viable nodes that could realistically result in a collision.

In order to identify whether a conjunction happens for every potential conjunction node, Kepler's equation is iteratively solved to compute the eccentric anomaly (E) for

each satellite from the node. Kepler's equation is typically written

$$E = M + e\sin(M), \tag{11}$$

where M is the mean anomaly and e is the eccentricity. Iteratively solving for E is achieved by

$$E_{n+1} = E_n - \frac{E_n - e\sin E_n - M}{1 - e\cos E_n} \tag{12}$$

until convergence. The angle ϕ, calculated in Eq. 8, is used to find the eccentric anomaly of each conjunction point.

$$E = 2\arctan\left(\sqrt{\frac{1-e}{1+e}}\tan\frac{\phi}{2}\right) \tag{13}$$

Then, those eccentric anomaly values are used to calculate the transit time between each satellite's starting position and arrival time at the conjunction point.

$$\tau = \frac{T}{2\pi}(E_c - E_0 - e(\sin E_c - \sin E_0)) \tag{14}$$

where T is the satellite's period, E_0 is the satellite's eccentric anomaly at the moment of assessment, and E_c is the eccentric anomaly of the conjunction point.

Given this transit time and a satellite's orbit, it is possible to generate a list of times when each satellite will arrive at the conjunction point. For example, if the transit time is $\tau = 500$ seconds, then the satellite will pass through the conjunction point 500 seconds after the start time. If that satellite has a period $T = 6{,}000$ seconds, then it will return to the conjunction point at 6,500 seconds, 12,500 seconds, 18,500 seconds, and so on. If a pair of satellites are both at the conjunction point at the same time (within some threshold Δt_{1-2}), then a conjunction has occurred.

One satellite may pass through many different conjunction nodes. Thus, it is necessary to sum the conjunction frequency across multiple nodes to compute a conjunction frequency for each satellite:

$$f_c^s = \sum_{i=1}^{n} f_c^n = \sum_{i=1}^{n} (T_{c_n})^{-1} \tag{15}$$

The satellite conjunction frequency directly relates to the operational criticality, capacity, and occupation. f_c^s itself represents a criticality score – a method for ranking the existing population of satellites by their interactions with other objects. Capacity is a threshold on the criticality, above which operations become infeasible. Occupation is identified by the ratio of f_c^s to the capacity threshold and gives an idea of whether a particular orbit is feasible or not for operations. Figure 3 shows a primary satellite (COSMOS 2058 in this

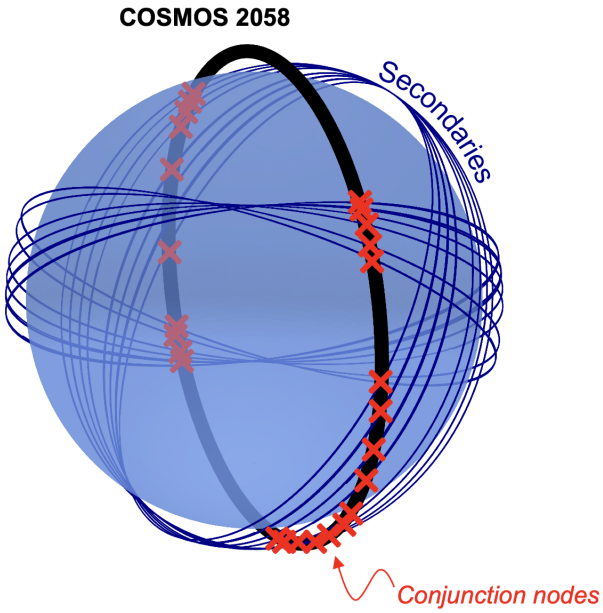

Fig. 3 Conjunction nodes for COSMOS 2058. COSMOS 2058's conjunction frequency is the sum of the nodal conjunction frequencies across all nodes.

case) and it's many conjoining secondary objects.

V. Results

The operationally feasible capacity framework is tested using the orbital elements for the entire tracked catalog of objects in LEO, as taken from the Two-Line Elements (TLEs) in October 2024. Every possible pairing of objects is evaluated. Orbital close approaches are identified for each pairing, and only close approaches with a node distance threshold of $\varepsilon \leq 100$ meters are considered viable conjunction nodes. T_c is computed for every combination of satellites that results in a viable conjunction node. Instances when $T_c < 0.2$ days are removed to screen out satellites that are in resonance and are de-conflicted by design. As a final check for each node, a search over one common period is performed to retain all conjunction nodes in which the satellites pass through the node within 1 s of each other. If no conjunction occurs within the common period, a conjunction between those objects in the near future is unlikely (according to the Keplerian assumption). Figure 4 shows the map of the remaining viable conjunction nodes based on this filtering process, along with the distribution of nodal conjunction frequencies across those nodes. A large majority of the conjunction nodes see $f_c^n < 2$ per month, but some approach 7 per month (not shown in the figure).

A high nodal conjunction frequency is achieved when an object pair has a low T_c and their orbit phases are not de-conflicted. Figure 5 shows the distribution of conjunction nodes in altitude and latitude. The large majority of the viable conjunction nodes fall near 400-600 km, a busy region in LEO occupied by the Starlink constellation ($\sim$7,000

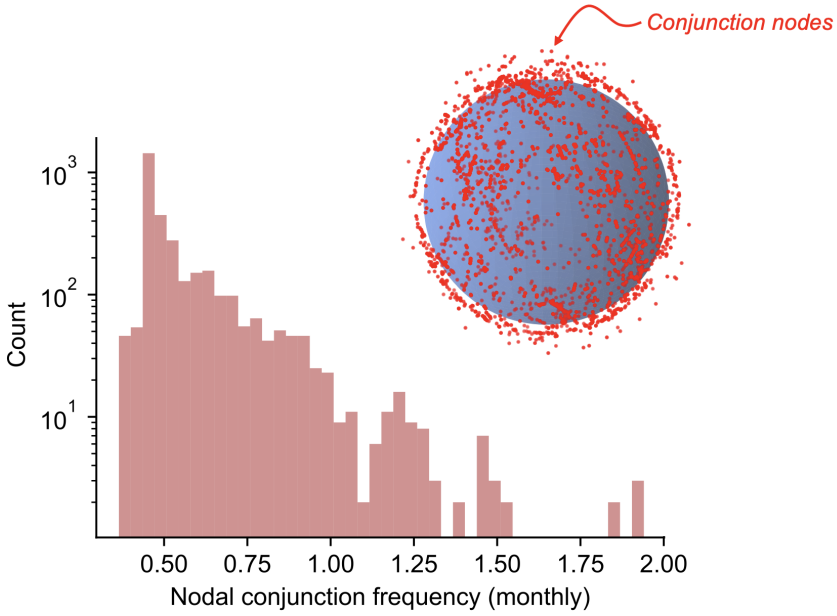

Fig. 4 Every conjunction node is assigned a nodal conjunction frequency, as determined by the inverse of T_c.

satellites) among many other commercial operators. It should be noted that of the viable conjunction nodes identified in this work, 77.7% involve at least one Starlink satellite, while only 3.7% involve Starlink-on-Starlink conjunctions. Intra-constellation conjunctions are rare because constellations are generally passively deconflicted so that, as long as the constellation is actively managed, satellites are phased in a way that they never conjoin. This architecture doesn't, however, protect against conjunctions with other objects traversing the same region in orbital space. Starlink satellites are involved in such a large portion of the conjunction nodes because they represent a large and multitudinous target for all other objects in orbit.

Figure 5(c) depicts a significant latitude dependence on conjunction node density. This distribution is explained by the fact that satellites spend the majority of their time in the extremities of their latitude bands. Major spikes at around $\pm 50^\circ$ and $\pm 82^\circ$ make sense since large satellite populations sit around inclinations that should peak there (Starlink and sun-synchronous satellites, respectively).

Figure 6 shows the cumulative density function (CDF) for the satellite conjunction frequency across the satellites under study. The large majority of those satellites see a low conjunction frequency the would not require regular maneuvers or mitigation actions. Notably, 67.5% of the 10,854 tracked objects see no conjunctions, and 0.27% (or 25 satellites) exceed the threshold of 10 conjunctions/month.

Table 1 reports the top 15 satellites ranked by conjunction frequency. Satellites achieve a high conjunction frequency when they are exposed to a large number of conjunction nodes, or a smaller number of high conjunction frequency nodes, or both.

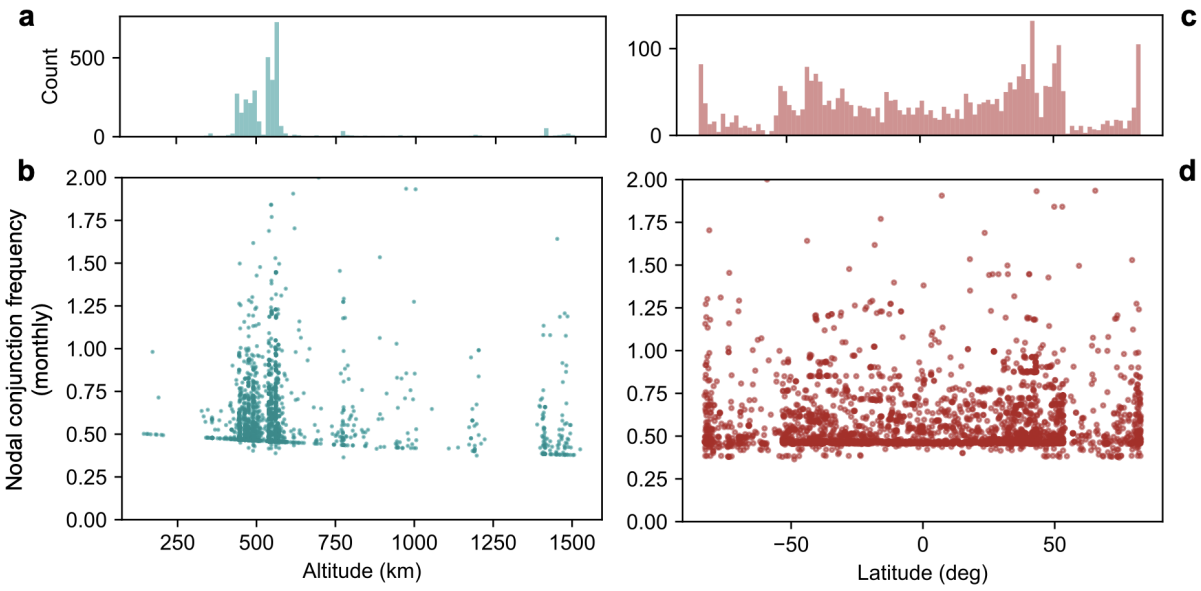

Fig. 5 Conjunction node distributions across (a, b) altitude and (c, d) latitude.

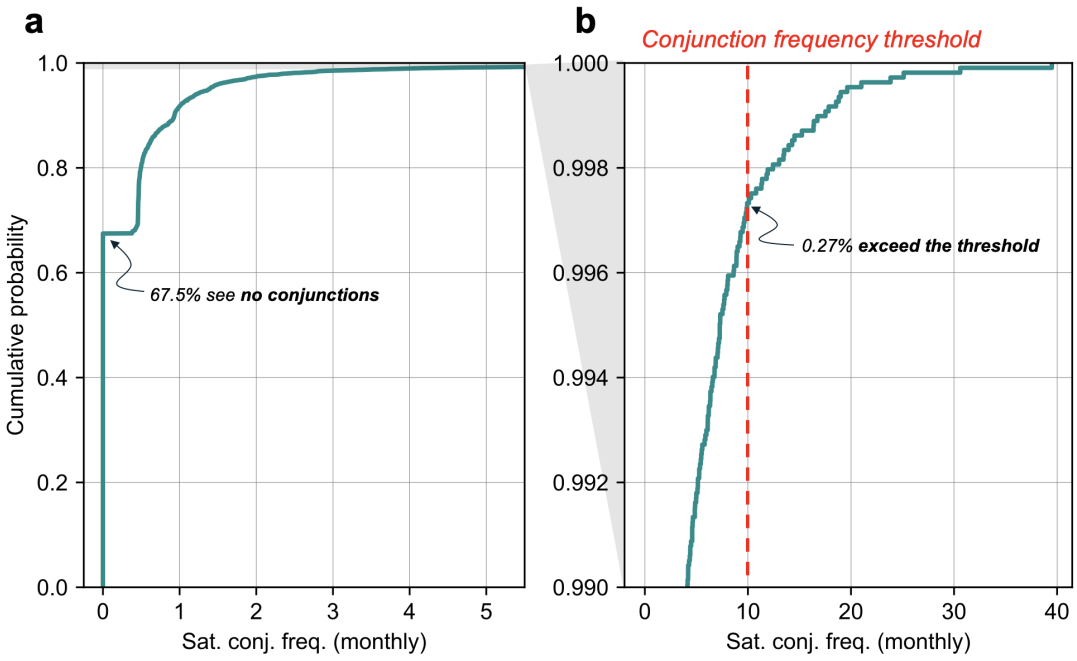

Fig. 6 Cumulative density function for satellite conjunction frequency. (a) shows the full CDF with a cutoff on the conjunction frequency, while (b) shows the top 1% of satellites by conjunction rate.

Figure 7 depicts these top 15 satellites' altitude range and conjunction altitudes. Most of the top conjunction rate objects sit between 520 and 580 km, except for Starlink-1096 (rank 13). A propulsion system failure rendered Starlink-1096 non-maneuverable, which led it to experience a large number of conjunctions around 440 km, where it currently sits. The Starlink constellation dominates the secondary object list for these top 15 conjunction frequency satellites. Table 2 in the appendix shows the secondary object list for the top 5 satellites, as well as Starlink-1096 (which, notably, interacts with a shell of other Starlink satellites near 440 km). Operating in such close proximity to a constellation without being de-conflicted by design means that many conjunction nodes are likely to form.

Table 1 Top 15 satellites by conjunction frequency

Rank	Name	NORAD ID	Conj. Nodes	f_c^s (monthly)
1	SHIJIAN 6 04A (SJ-6 04A)	37179	64	39.4929
2	TIANQI-14	48864	67	30.5994
3	UPPER FREE FLYER	43763	29	25.1128
4	COSMOS 2058	20465	28	23.8404
5	GEESAT 3-09	61019	43	21.0055
6	SHIJIAN 6 01B (SJ-6 01B)	28414	41	19.6351
7	EXCITE	43819	20	19.0006
8	NANOSAT C BR1	40024	41	18.8160
9	CORVUS BC1	42847	35	18.5570
10	TK-2	52150	28	17.8379
11	AO-95	43770	38	17.5217
12	CSC-1	58022	27	16.7452
13	STARLINK-1096	44942	35	16.3957
14	R2	46913	35	16.3648
15	LEMUR 2 FURIAUS	42840	32	15.2398

VI. Discussion and Conclusion

This work sought to model the satellite-carrying capacity of Earth's orbit based on an operational feasibility constraint. The goal of this effort was not to define a maximum number of satellites that the environment could sustain, but rather to identify clear operator-centric constraints that determine whether a capacity threshold has been crossed for an orbit of interest. The maximum acceptable conjunction rate per satellite was set to 10 conjunctions per month. Beyond this limit, the risk or maneuver burden on an operator is deemed too great to justify operating in that orbit.

The assumption of Keplerian dynamics was important for enabling analytical meth-

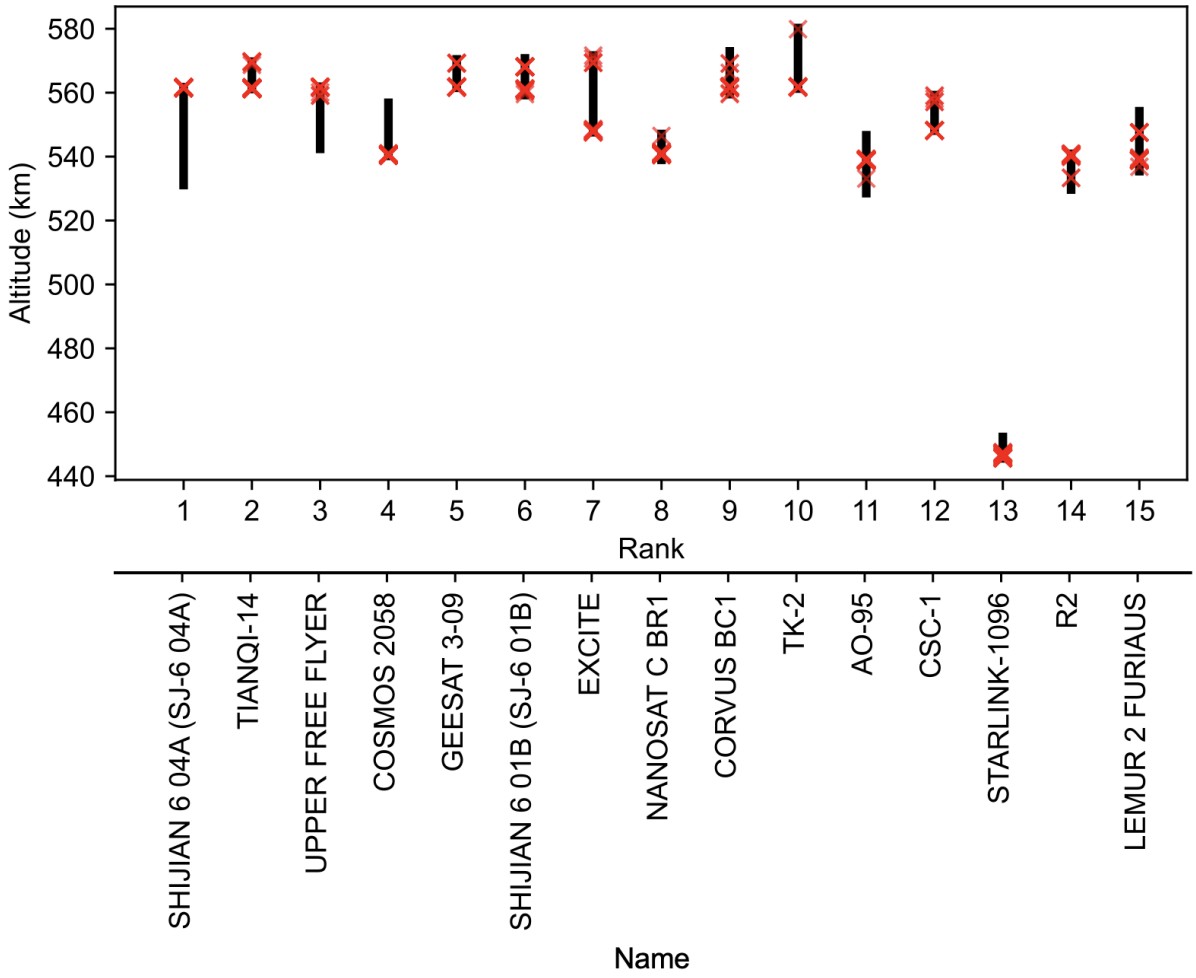

Fig. 7 Visualization of the altitude range for the top 15 satellites by conjunction frequency. Large constellations like Starlink and OneWeb represent the majority of secondary objects in the conjunctions.

ods for computing conjunction node geometry and frequency. However, the simplification of the dynamics means that actual trajectories for the objects under study will vary, especially over longer time periods when Earth's complex gravity field and drag in LEO will significantly perturb satellite trajectories. This higher fidelity analysis will be the subject of future work, though this analysis framework should hold for the higher fidelity propagation.

From this work, it appears the majority of existing tracked object orbits (99.73% of LEO) do not appear to exceed the 10 conjunction/month capacity threshold. Yet 25 objects were identified as exceeding this threshold – with secondary objects in those conjunctions dominated by the Starlink constellation. While the satellite conjunction frequency is useful for assessing occupation (how much of the available capacity for a trajectory has been occupied) it also serves as a useful criticality metric. Satellites identified as having high conjunction frequencies see regular interactions with other objects that could result in a bothersome maneuver burden or even a potential collision

if left unchecked. Satellites with especially high conjunction frequencies are worrisome.

Structure plays a major role in determining the number of satellites that may sustainably operate within a region of interest. Constellations generally do a good job at densely packing satellites within a small volume and limiting conjunctions through passively de-conflicted orbit design. While the structure of constellations helps to prevent intra-constellation conjunctions, it does not protect against conjunctions with other objects. The results of this work showed that the majority of conjunction nodes involve at least one Starlink satellite, and the top satellites by conjunction frequency are almost exclusively interacting with Starlink.

The orbits of the top satellites by conjunction frequency have not reached capacity due to their own actions or presence. Most were launched prior to Starlink, and only became oversaturated after the large constellation entered their orbital domain. Historically, Starlink has taken maneuver responsibility for most conjunctions with external objects, which should free up those satellites from the maneuver burden with Starlink secondaries. Yet, a lack of regulatory oversight in the collision avoidance maneuvering process makes it difficult to rely on this dynamic to continue indefinitely. Even if a large operator guarantees that they will always take maneuver responsibility, conjunction assessment is imperfect (especially during solar maximum and geomagnetic storms) and collision avoidance maneuvers will never eliminate risk entirely.

Removing the high-conjunction rate satellites from orbit may indeed efficiently reduce aggregate collision risk, but it is important to remember that the risk was introduced by a single large operator disrupting existing traffic. While space traffic coordination and management is essential, it should not be dictated by large constellations staking claims in LEO and displacing other operators. A fairer, more deliberate approach is possible and should be sought out.

The decisions made by any single operator in Earth's orbit can have significant impacts on the operational feasibility of all other spacecraft nearby. The recent rapid commercialization and expansion of space activities threatens the long term sustainability of operations in space. In order to ensure that space remains operationally useful for generations to come, it is important that we understand how to measure, apportion, and coordinate access to space for the benefit of all.

VII. Appendix

Table 2 Secondary objects for high conjunction frequency primary satellites (S = Starlink).

Rank	Secondary Objects
1	S-5304, S-5087, S-5407, S-5405, S-6120, S-5090, S-30106, S-30083, S-6189, S-6157, S-6173, S-6176, S-6273, S-6277, S-6267, S-6283, S-5136, S-6260, S-6261, S-6224, S-5335, S-5348, S-5342, S-5346, S-6337, S-6280, S-6310, S-6314, S-6226, S-6187, S-6199, S-30151, S-30135, S-30136, S-5845, S-5860, S-30206, S-30288, S-30333, S-30349, S-30281, S-30365, S-30343, S-30359, S-30759, S-30783, S-30761, S-30775, S-30806, S-30778, S-30830, S-30845, S-30805, S-30851, S-30792, S-30840, S-31020, S-31015, S-31023, S-31001, S-31009, S-31094, S-31180, S-31042
2	S-5382, S-5394, S-5389, S-5082, S-5087, S-5084, S-5400, S-5633, S-5618, S-5030, S-5615, S-5643, S-6091, S-6117, S-6071, S-5566, S-5375, S-30084, S-30114, S-30151, S-5881, S-6223, S-6217, S-5536, S-5832, S-5828, S-5838, S-5542, S-6194, S-6184, S-6247, S-6262, S-6225, S-6235, S-30286, S-30345, S-30300, S-30334, S-30768, S-30787, S-30770, S-30806, S-30778, S-30801, S-30830, S-30827, S-30762, S-31001, S-30988, S-5689, S-5690, S-5692, S-5695, S-5344, S-5365, S-5748, S-5500, S-5579, S-5611, S-5900, S-5808, S-30155, S-30161, S-30176, S-30495, S-30498, S-30503
3	S-4461, S-4448, S-5957, S-5940, S-5949, S-5777, S-5792, S-6177, S-6207, S-6195, S-6098, S-5519, S-30213, S-30174, S-30328, S-30324, S-30247, S-30538, S-30597, S-30551, S-30590, S-30574, S-30919, S-30955, S-30908, S-30969, S-30991, S-31002, S-5967
4	S-3200, S-3632, S-3557, S-3539, S-3568, S-3567, S-3647, S-3538, S-3964, S-3948, S-3953, S-3924, S-3895, S-3922, S-3906, S-3867, S-3936, S-4078, S-4207, S-4298, S-4534, S-4515, S-4512, S-4525, S-4491, S-5290, S-5122, S-5250
5	S-5416, S-5882, S-5889, S-5894, S-5905, S-5948, S-5944, S-5789, S-5801, S-5803, S-30084, S-30128, S-30135, S-5853, S-6098, S-6179, S-5961, S-5966, S-5952, S-5733, S-5746, S-6229, S-30252, S-30329, S-30324, S-30345, S-30346, S-30300, S-30334, S-30538, S-30497, S-30525, S-30598, S-30551, S-30590, S-30608, S-30574, S-30925, S-30979, S-31005, S-31023, S-5634, S-5923
13	S-31590, S-31567, S-31282, S-31632, S-31473, S-31396, S-31568, S-31415, S-31617, S-31621, S-31742, S-31650, S-31679, S-31453, S-31513, S-31624, S-31689, S-31880, S-31910, S-31854, S-31875, S-32080, S-32091, S-32103, S-32090, S-32102, S-32093, S-31817, S-31821, S-31726, S-31681, S-31783, S-31893, S-31676, S-31960

Data Availability

No datasets were generated or analyzed during the current study.

Code Availability

The code developed in this work is provided in `https://github.com/ARCLab-MIT/operational_capacity`.

Acknowledgments

Research was sponsored by the Department of the Air Force Artificial Intelligence Accelerator and was accomplished under Cooperative Agreement Number FA8750-19-2-1000. The views and conclusions contained in this document are those of the authors and should not be interpreted as representing the official policies, either expressed or implied, of the Department of the Air Force or the U.S. Government. The U.S. Government is authorized to reproduce and distribute reprints for Government purposes notwithstanding any copyright notation herein.

References

[1] Del Monte-Luna, P., Brook, B. W., Zetina-Rejón, M. J., and Cruz-Escalona, V. H., "The carrying capacity of ecosystems," *Global ecology and biogeography*, Vol. 13, No. 6, 2004, pp. 485–495.

[2] Letizia, F., Virgili, B. B., and Lemmens, S., "Assessment of orbital capacity thresholds through long-term simulations of the debris environment," *Advances in Space Research*, Vol. 72, No. 7, 2023, pp. 2552–2569.

[3] McKnight, D., Dale, E., Patel, M., and Kunstadter, C., "Modeling Empirical Orbital Capacity," *Space capacity allocation for the sustainability of space activities workshop, Politecnico di Milan*, 2023.

[4] D'Ambrosio, A., and Linares, R., "Carrying Capacity of Low Earth Orbit Computed Using Source-Sink Models," *Journal of Spacecraft and Rockets*, 2024, pp. 1–17.

[5] Jang, D., "Modeling the Future Space Debris Population and Orbital Capacity," Ph.D. thesis, Massachusetts Institute of Technology, 2024.

[6] Rothblatt, M. A., "Satellite communication and spectrum allocation," *American Journal of International Law*, Vol. 76, No. 1, 1982, pp. 56–77.

[7] Eggl, S., Benkhaldoun, Z., Micheva, G., Spencer, S. T., Stark, D. V., Winkel, B., Rawls, M., and Peel, M. W., "SatHub Panel: Satellite Interference in Observatories Around the World," *arXiv preprint arXiv:2408.15222*, 2024.

[8] Ailor, W., and Patera, R., "Spacecraft re-entry strategies: meeting debris mitigation and ground safety requirements," *Proceedings of the Institution of Mechanical Engineers, Part G: Journal of Aerospace Engineering*, Vol. 221, No. 6, 2007, pp. 947–953.

[9] Dallas, J., Raval, S., Gaitan, J. A., Saydam, S., and Dempster, A., "The environmental impact of emissions from space launches: A comprehensive review," *Journal of Cleaner Production*, Vol. 255, 2020, p. 120209.

[10] Ferreira, J. P., Nomura, K., and Wang, J., "Preliminary assessment of the environmental impact of space debris demise during atmospheric reentry," *Advanced Maui Optical and Space Surveillance Technologies (AMOS) Conference*, 2023.

[11] NASA, "NASA Space Sustainability Strategy," , March 2024. URL `https://www.nasa.gov/wp-content/uploads/2024/04/nasa-space-sustainability-strategy-march-20-2024-tagged3.pdf?emrc=676978822fa0b`, accessed: February 4, 2025.

[12] United Nations Framework Convention on Climate Change (UNFCCC), "The Paris Agreement," , 2015. URL `https://unfccc.int/process-and-meetings/the-paris-agreement`, accessed: February 4, 2025.

[13] Rossi, A., Valsecchi, G. B., and Alessi, E. M., "The Criticality of Spacecraft Index," *Advances in Space Research*, Vol. 56, No. 3, 2015, pp. 449–460. https://doi.org/10.1016/j.asr.2015.02.027.

[14] Letizia, F., Lemmens, S., Bastida Virgili, B., and Krag, H., "Application of a Debris Index for Global Evaluation of Mitigation Strategies," *Acta Astronautica*, Vol. 161, 2019, pp. 348–362. https://doi.org/10.1016/j.actaastro.2019.05.003.

[15] Servadio, S., Simha, N., Gusmini, D., Jang, D., St. Francis, T., D'Ambrosio, A., Lavezzi, G., and Linares, R., "Risk Index for the Optimal Ranking of Active Debris Removal Targets," *Journal of Spacecraft and Rockets*, Vol. 0, No. 0, 0, pp. 1–14. https://doi.org/10.2514/1.A35752.

[16] Letizia, F., Lemmens, S., Virgili, B. B., and Krag, H., "Application of a debris index for global evaluation of mitigation strategies," *Acta Astronautica*, Vol. 161, 2019, pp. 348–362.

[17] Parker, W., Brown, M., and Linares, R., "Greenhouse G=gases reduce the satellite carrying capacity of low Earth orbit," *Nature Sustainability*, 2025.

[18] Talent, D., "Analytical model for orbital debris environmental management," *AIAA*, 1990. URL https://ntrs.nasa.gov/citations/19900045002.

[19] Lewis, H. G., Swinerd, G. G., Newland, R. J., and Saunders, A., "The fast debris evolution model," *Advances in Space Research*, Vol. 44, 2009, pp. 568–578. https://doi.org/10.1016/j.asr.2009.05.018.

[20] JASON report, “The Impacts of Large Constellations of Satellites,” , 2020.

[21] Somma, G. L., “Adaptive remediation of the space debris environment using feedback control,” Ph.D. thesis, University of Southampton, 2019.

[22] Kebschull, C., Radtke, J., Krag, H., Agency, E. S., and Assessment, D. R., “Deriving a priority list based on the environmental criticality,” *Proceedings of the 65th International Astronautical Congress*, International Astronautical Federation, Toronto, Canada, 2014.

[23] D’Ambrosio, A., Servadio, S., Mun Siew, P., and Linares, R., “Novel Source–Sink Model for Space Environment Evolution with Orbit Capacity Assessment,” *Journal of Spacecraft and Rockets*, Vol. 60, No. 4, 2023, pp. 1112–1126. https://doi.org/10.2514/1.A35579.

[24] Lifson, M., Jang, D., and Linares, R., “Space Environmental Governance and Decision Support using Source-Sink Evolutionary Environmental Models,” *24th Advanced Maui Optical and Space Surveillance Technologies*, Maui Economic Development Board, Maui, HI, 2023.

[25] Tian, R. M., Xi, K., Lavezzi, G., Lifson, M., Servadio, S., and Linares, R., “Optimizing Active Debris Removal Strategies With Feedback Control For A Sustainable Space Environment,” *AAS/AIAA Astrodynamics Specialist Conference*, Broomfield, CO, 2024.

[26] Brownhall, I., Lavezzi, G., Jang, D., Lifson, M., Bhattarai, S., and Linares, R., “A Flexible and Improved Source Sink Evolutionary Model to Support Transdisciplinary Orbital Capacity Analysis,” *75th International Astronautical Congress*, Milan, Italy, 2024. https://doi.org/10.52202/078360-0091.

[27] Liou, J. C., Hall, D. T., Krisko, P. H., and Opiela, J. N., “LEGEND – a Three-dimensional LEO-to-GEO Debris Evolutionary Model,” *Advances in Space Research*, Vol. 34, 2004, pp. 981–986. https://doi.org/10.1016/J.ASR.2003.02.027.

[28] Lewis, H., Swinerd, G., Williams, N., and Gittins, G., “DAMAGE: a Dedicated GEO Debris Model Framework,” *3rd European Conference on Space Debris*, 2001, pp. 373–378.

[29] Lewis, H. G., Saunders, A., Swinerd, G., and Newland, R. J., “Effect of thermospheric contraction on remediation of the near-Earth space debris environment,” *Journal of Geophysical Research: Space Physics*, Vol. 116, 2011. https://doi.org/10.1029/2011JA016482.

[30] Dolado-perez, J., Di Costanzo, R., and Revelin, B., “Introducing Medee-a New Orbital Debris Evolutionary Model,” *Proc. 6th European Conference on Space Debris*, 2013, pp. 22–25.

[31] Martin, C. E., Cheese, J. E., and Klinkrad, H., “Space Debris Environment Analysis with DELTA 2.0,” *International Astronautical Federation - 55th International Astronautical Congress 2004*, 2004. https://doi.org/10.2514/6.IAC-04-IAA.5.12.5.04.

[32] Radtke, J., Mueller, S., Schaus, V., and Stoll, E., "LUCA2 - An enhanced long-term utility for collision analysis | ESA Proceedings Database," 2017.

[33] Sorge, M. E., and Mains, D. L., "IMPACT Fragmentation Model Improvements," *AIAA/AAS Astrodynamics Specialist Conference*, 2014. https://doi.org/10.2514/6.2014-4228.

[34] Wang, X. W., and Liu, J., "An Introduction to a New Space Debris Evolution Model: SOLEM," *Advances in Astronomy*, Vol. 2019, 2019. https://doi.org/10.1155/2019/2738276.

[35] Drmola, J., and Hubik, T., "Kessler Syndrome: System Dynamics Model," *Space Policy*, Vol. 44-45, 2018, pp. 29–39. https://doi.org/10.1016/J.SPACEPOL.2018.03.003.

[36] Rosengren, A. J., Skoulidou, D. K., Tsiganis, K., and Voyatzis, G., "Dynamical cartography of Earth satellite orbits," *Advances in Space Research*, Vol. 63, 2019, pp. 443–460. https://doi.org/10.1016/J.ASR.2018.09.004.

[37] Jang, D., Gusmini, D., Siew, P. M., D'Ambrosio, A., Servadio, S., Machuca, P., and Linares, R., "A New Monte-Carlo Model for the Space Environment," , 2024.

[38] Parker, W., and Linares, R., "Satellite Drag Analysis During the May 2024 Gannon Geomagnetic Storm," *Journal of Spacecraft and Rockets*, Vol. 61, 2024, pp. 1–5. https://doi.org/10.2514/1.A36164.

[39] Acedo, L., "Kinematics effects of atmospheric friction in spacecraft flybys," *Advances in Space Research*, Vol. 59, No. 7, 2017, pp. 1715–1723. https://doi.org/https://doi.org/10.1016/j.asr.2017.01.008.

[40] Bowman, B., Tobiska, W. K., Marcos, F., Huang, C., Lin, C., and Burke, W., "A new empirical thermospheric density model JB2008 using new solar and geomagnetic indices," *AIAA/AAS astrodynamics specialist conference and exhibit*, 2008, p. 6438.

[41] Alfano, S., and Finkleman, D., "On selecting satellite conjunction filter parameters," *Acta Astronautica*, Vol. 99, 2014, pp. 193–200.